PREDICTIONS OF KUMAMOTO GROUND MOTION FROM LINEAR AND NONLINEAR 2D SIMULATION IN THE FRAMEWORK OF EGS STEP 2 AND STEP 3 BLIND TEST

Bordoni P.[1], Milana G.[1], Lucarelli A.[2], Di Giulio G.[1], Hailemikael S.[3], Vassallo M.[1]
1 Istituto Nazionale di Geofisica e Vulcanologia (paola.bordoni@ingv.it, giuliano.milana@ingv.it, giuseppe.digiulio@ingv.it, maurizio.vassallo@ingv.it)
2 Itasca Consulting (alucarelli@itascacg.com)
3 ENEA (salomon.hailemikael@enea.it)

ABSTRACT

We present the results of 2D numerical simulation carried out using FLAC3D-7.0. The model geometry has been derived by the seismic section provided by the ESGG6 organizing committee (CMPM) and by the Japan Integrated Velocity Structure Model (JIVSM). The seismic velocity model and density were derived from the 1D preferred model proposed by CMPM for the units filling the Kumamoto Plain, and from the JIVSM for the Mount Kinbo area.
We have performed an elastic simulation for Step2, while for Step3, in addition to a linear elastic simulation, a non-linear elasto-plastic simulation has been run using the Mohr-Coulomb constitutive law to characterize some shallow layers. For Step3 linear and nonlinear synthetics waveforms are almost identical, likely due to the mechanical parameters and the constitutive model chosen being not able to induce non-linear effects. Synthetic results are presented for horizontal and vertical components of ground motion.

Keywords: ESG6, Kumamoto, Japan, 2d modeling, finite difference technique, nonlinear behavior, blind prediction

INTRODUCTION

We have welcomed the invitation of the local organizing committee of EGS6 to participate as analysts in the 2020 blind predictions. The Step 1 results are presented in a companion paper (Di Giulio et al., 2021), while another companion paper (Hailemikael et al., 2021) illustrates our 1D modeling predictions. Here we present predictions done by 2D numerical simulation: Step 2 for the simulation of weak motion as well as Step 3 for the simulation of strong motion. On the basis of the limited available data we decided to build a simple 2D model, with plane parallel geometry around the target site, likely very far from the complexity of the real geology hidden below the Kumamoto plain.
The plain indeed (Figure 1) extends across the northeastern part of the Kumamoto Prefecture from the western slope of Mt Aso to Ariake Bay and it is formed by the alluvial deposits of the Shirakawa and Midorikawa rivers draining towards Ariake Bay. The target site (KUMA) is very close to the sharp bend of the Shirakawa river in Kumamoto City. The geology of Kumamoto city comprises alluvium deposits by the Shirakawa River, andesite rocks deposited around Mt. Kinbo and Mt. Aso pyroclastic sequence of flow deposits (Tsuno et al. 2017), such as Aso-1 to Aso-4 which are younger from the Aso-1 to the Aso-4. Between the Aso-4 and Aso-3 deposits the Miyuki Formation have been found (Ishizaka et al. 1995, Nakazawa et al. 2018), with lithofacies ranging from basal gravel to a middle horizon of marine clay to upper gravel, interpreted as buried marine terrace deposits (Ishizaka et al. 1995). Therefore, the subsoil geology of the plain is a complex result of the interplay between tectonics, glacio-eustatic sea-level changes, and subsidence.
The average shear-wave velocity down to 30 m is reported by the Japanese Seismic Hazard Information Station (Headquarters for Earthquake research promotion, Cabinet office, Government of Japan 2005) ranging from 155 to 405 m/s on the Kumamoto plain and a value of 510 m/s on Mt Kimbo suggesting a possible role of ground motion amplification in the area. Despite all that, only slight damage to buildings had been caused by the 2016 Kumamoto earthquake sequence with intensity values of the Japanese intensity scale of about 6 even if Kumamoto city is located only at about 15 Km from the earthquake source. Conversely, the earthquake sequence produced high damage eastern of Kumamoto city, in

Mashiki, where the maximum intensity value of the Japanese intensity scale was recorded (i.e. 7) and where on top of the Aso-4 deposits very slow lahar deposits have been found (Nakazawa et al. 2018).

NUMERICAL SIMULATION METHOD

The 2D simulation was performed using the FLAC3D-7.0 code (Itasca Consulting Group, Inc. (2019). FLAC3D (Fast Lagrangian Analysis of Continua in 3 Dimensions) is a numerical modeling software for geotechnical analyses that utilizes an explicit finite volume formulation. The software simulates the nonlinear behavior of soil based on constitutive models which describe the response behavior of materials under different mechanical conditions. FLAC3D can be used to run bi-dimensional modeling in addition to the three-dimensional and, due to the limited available information provided for this exercise, we decided on the 2D modeling option setting a minimum width of 2 m in the y-direction.
The FLAC3D solving algorithm is based on the finite difference method and requires the realization of a spatial grid to discretize the domain. We have chosen the structured grid approach selecting a solving grid with a brick shape of 13 meters in the x-direction, 10 meters in the z-direction and 2 m in the y-direction. We have then used up to 3 densification levels depending on the investigated materials. In particular the brick size was reduced to 1) 1.6x1.25x2 meters down to 60 m; 2) 3.25x2.5x2 down to 100 m; and 3) 6.5x5x2 down to 200 m. The selected grid size allows the recovery of signals at frequency up to 10 Hz in the x direction (see Table 2 for details). An absorbing boundary (quiet boundary) was applied at the bottom of the model to reduce the effect of multiple reflections at its base. Spurious reflections due to the lateral model boundaries are minimized applying a free field condition both in the horizontal and vertical directions.
The Step 2 target earthquake is from April 16, 2016 at 03:03 (Mj=5.9). The Step 3 target earthquake is the Mj 6.4 foreshock of the Kumamoto earthquake of 2016/04/14/21:26 JST. In both cases the recording at SEVO has been used as input motion at the base of the model after having removed the free surface effect simply dividing the original waveform by two.
Each simulation was performed applying simultaneously horizontal and vertical components acting at the model base with a vertical incidence. In our approach we performed 2 simulations for each event using as input: 1) EW and UP components in one case and 2) NS and UP components in the other.
For both computations, the input signal was of 4600 points with a constant time sampling of 0.01 s, resulting in a duration of 46.00 seconds for both the horizontal and vertical components. The original input signals were cut about 5 seconds before the P wave arrival time picked on the vertical component of the SEVO records.The input data were corrected removing the average value of the records and high pass filtered at 15 Hz to avoid artefacts related to the grid size used in the simulation. When using a quiet boundary FLAC3D requires the input data to be expressed in velocity so no integration was necessary on the original time series that were uploaded in m/s units.

SUBSURFACE MODEL

Geometry and Mechanical parameters

The 2D geometry of our model was derived by the geological interpretation of the seismic reflection cross-section presented in Figure 2, redrawn from the Figure 15 of the Report furnished by CMPM (*https://www.jishin.go.jp/main/chousakenkyuu/kumamoto_sogochousa/h28/h28kumamoto_sogochousa_3_2.pdf*). The cross-section shows four seismic discontinuities under the Kumamoto plain. Below the Kumamoto plain, which has a width of about 9000 m, the seismic survey has detected a basin structure carved into the Cretaceous basement, the Mifune Formation, corresponding to the third reflective surface. Indeed, this third seismic reflection plane can clearly be traced from the ground surface close to the South tip of the survey line, where the chalk Mifune Group formation outcrops, to a depth of about 400 meters below CMP 2200 m and extends toward the North reaching a maximum depth of about 600 m below CMP 1200. In the area between CMP 2200 and CMP 2400, it is evident the Futagawa Fault Zone Uto section (Uto fault) as described by the Headquarters for Earthquake Research Promotion (2013). It has been confirmed that the reflection surface corresponding to the upper surface of the chalk basement rock is inclined to the north. On the other hand, as shown in the geological interpretation map (Figure 2), faults of the normal fault system are estimated from the morphology of the reflecting surface near CMP1600 and CMP2150. The vertical displacement of each fault is estimated to be several tens of

meters in the Aso pyroclastic flow deposit. However, the deformation of the upper surface of the basement rock is not clear. Another fault, the Tatsudayama fault, passes near CMP200 according to the Kumamoto geological map (1 / 100,000), but no clear reflection surface showing the fault structure is observed. Our model does not include either of the described faults because it extends from CMP 400 to CMP 1200, and the prediction site is close to CMP 1000 (Figure 2). Near the North tip of the survey line, the basement rocks belonging to Mt. Kinbo and Otaka pre-Aso volcanic rock are distributed from just below the ground surface. It is estimated that metamorphic rocks and granites constitute the deep basement under these rocks. The first and the second reflection surfaces have been traced on the basis of existing bore-hole logs where the basal strata Aso-3 and Aso-1 were estimated. The deposit between the Aso-1 and upper surface of the Mifune formation has been associated with the Suizenji Formation (Hase and Iwauchi 1992) which has about 300 m thickness close to CMP 1200. The fourth seismic discontinuity is associated with the top of the basement rocks. The superficial deposits are characterized by Ariake clays formation deposited over the Aso-4 to Aso-1 pyroclastic flow. Between the Aso-4 and Aso-3 deposits the Miyuki Formation has been found (Ishizaka et al. 1995, Nakazawa et al. 2018) (*https://www.jishin.go.jp/main/chousakenkyuu/kumamoto_sogochousa/h28/h28kumamoto_sogochousa_3_2.pdf*). To define the velocity-depth model we have divided the cross-section into two sectors: a basin area filled by the sedimentary units deposited in the Kumamoto plain (Plain Model, PM), and an area characterized by the volcanic units of Mount Kinbo (Kinbo Model, KM). The velocity, density and thickness for PM were derived from the 1D preferred model furnished by CMPM, while for KM, the values were inferred from the Japan Integrated Velocity Structure Model (JIVSM) (Koketsu et al., 2009; 2012). The bedrock unit was common to both model sectors and derived by CMPM. The PM area was divided into 9 layers, mostly plane parallels, and the KM into 5 layers with their geometry interpreted from a cross section extrapolated from JIVSM. Velocity, density and Poisson ratio values are obtained by grouping and averaging the velocity values provided by CMPM and by JIVSM (see Table 3 and Table 4). The model section is shown in Figure 2 superimposed to the seismic section for reference. It extends for 4.0 Km laterally and for 1.5 Km in depth. The prediction site is located 3200 meters from the left edge of the section, at CMP 1000, where synthetic time histories of acceleration and strain have been evaluated.

Constitutive models

To define the dynamic behavior of soil, FLA3D requires a constitutive model to be assigned to each layer (defined selecting and grouping specific areas of the brick model) as well as shear modulus degradation curves (G/G0). For the weak seismicity Step 2 we have assumed a damped elastic behavior for all the layers. For the strong motion Step 3, to describe nonlinear soil behavior, the shallow PM layers “plain1”, “plain2”, “plain3” are assigned to Mohr-Coulomb constitutive model (MC) while we have assumed an elastic behavior for all KM layers and for PM layers ranging from “plain4” down to “meta”. When the MC constitutive model is used, FLAC3D makes use of G/G0 curves only for low deformation levels, while MC model steps in when the deformation increases. The G/G0 variation has been evaluated using the Darendeli approach (Darendeli, 2001) that considers the influence of depth in the nonlinear behavior for a given type of material. Both Darendeli and MC approaches require some parameters to describe the material behavior, which were not provided by CMPM. In such cases, based on the soil type furnished by CMPM (Oyo Corporation, 2020), we have selected the average values commonly used in geotechnical engineering practice. The density and damping factors applied to the elastic materials are shown in Table 3 and Table 4 while Table 5 lists the geotechnical parameters values required by MC approach. The damping can be considered frequency independent in the investigated frequency range.

Model calibration

The local committee released 12 weak ground motion data both at the reference site (SEVO) and at the prediction site (KUMA) which we used for testing and calibrating the prediction capabilities of our model. This step was done using a fully elastic constitutive law in line with Step 2 requirements. The damping value adopted in the modeling was derived from a parametric analysis performed using the event No. 206 located close to the target earthquake proposed in Step 2 whose horizontal components of motion were similar. For these events the epicentral distance to KUMA and SEVO site are very similar, allowing us to use the records provided without applying any correction for distance. In

particular, we tried to fit the experimental spectral ratio between the records collected at KUMA and SEVO stations both on horizontal and vertical components, assuming SEVO as a rock reference site.
Therefore, we considered our model good enough when the predicted spectral ratios match the experimental spectral ratio of event # 206 from both the horizontal and the vertical components of motion (see Figure 3). This holds true for Step 2 predictions, while for Step 3, when nonlinearity steps in, it might not be so appropriate. But considering the little constraints we have, it was an acceptable starting point for Step 3. The parametric approach has been useful to select a good (in the terms previously defined) damping curve (Figure 4), using the "Maxwell" damping approach (Bielak et al., 2011; Dawson and Cheng, 2021, in press) based on a spring in series with a dashpot.
In Step 3, to explore how different constitutive models can describe the behaviour of strong motion shaking we run a linear elastic simulation and a non-linear elasto-plastic simulation.

RESULTS

Predicted ground motions do not show a relevant site dependent variability along the cross section for recording sites located away from the Kumamoto basin edges close to the target site, likely due to the simple plane parallel geometry we have reconstructed around the prediction site, but the 2D modeling is still useful for predicting a relevant motion in the vertical component. The results of simulation are shown for Step2 in Figures 5 (E-W and U-D components) and Figures 6 (N-S and U-D components) in terms of synthetics acceleration waveforms, and in Figure 7 in terms of synthetic Fourier spectra. For Step 3 the results are shown from Figure 8 to Figure 10, with the same contents order. The obtained PGA values are: for Step 2 of 0.7 m/s^2 and 0.08 m/s^2 on horizontal and vertical components respectively, and for Step 3 of about 4.5 m/s^2 and 1.6 m/s^2 on horizontal and vertical components respectively. Step 2 N-S horizontal component of motion has a PGA bigger than the E-W one of about 0.3 while Step 3 horizontal components are of the same order of magnitude, reflecting the signal input differences. As required by the Blind test exercise, we have evaluated the maximum shear-strain versus depth for the Mj=5.9 and Mj=6.4 for both EW and NS components. Figure 9 shows results down to a depth of 150 meters. For both types of simulations, the maximum strain is reached at a depth of about 10 m with a value of about 0.022% (Step2) and 0.16% (Step3). At depths more than 150 meters the strain decreases rapidly reaching at the base of the model values lower than 10^{-4} for Step2, and 10^{-3} and Step3 simulation. Quite surprisingly to us, the Step 3 results do not change when using an elastic constitutive law with the same Maxwell damping in substitution of the Mohr-Coulomb constitutive model associated with Darendeli degradation curve and a Maxwell damping. Figure 12 shows the closeness of the stress-strain relationship produced by the elastic linear and the elasto-plastic non-linear approaches indicating that the plasticity threshold is not reached.

CONCLUSIONS

Synthetics seismograms produced by linear and non-linear 2D numerical simulation for the Step 3 Mj=6.4 are almost identical, despite having assigned to the first 3 layer of the models, down to a depth of about 30 m, a Mohr-Coulomb constitutive model and a Darendeli modulus degradation curve. This came as a little surprise to us since the level of strain developed in the first 10 m of model depth reached about the same level of strain (0.0016) produced by the 1D linear equivalent STRATA and nonlinear DEEPSOIL codes (Hailemikael et al., 2021) and where nonlinearity shows its effect clearly changing the frequency content and the amplification level of the spectra. The stress-strain relationship produced by our Step3 model (Figure 12) does not show a significant difference between the linear and non-linear approaches supporting the observation made on the obtained synthetic waveforms.
We have inferred therefore that the mechanical parameters used to characterize the soil behavior as well as the constitutive model chosen are not able to induce non-linear effects, at least in the frequency range we have studied (0-10 Hz). The PGA produced by Step3 simulation is about 447 gal, and this value is higher than the PGA limit (150 gal) indicated by Tsuno et al. (2017) as the threshold between linear and non-linear behavior during Kumamoto sequence.

REFERENCES

Bielak, J., Karaoglu, H. and Taborda, R., (2011). "Memory-efficient displacement-based internal friction for wave propagation simulation". *Geophysics*, **76**(6), pp.T131-T145.

Darendeli M., (2001). "Development of a New Family of Normalized Modulus Reduction and Material Damping Curves" (Ph.D. dissertation). University of Texas at Austin, USA.

Dawson, E.M., and Z. Cheng (2021). "Maxwell damping, an alternative to Rayleigh damping", Draft paper for Geo-Extreme Conference, Savanah, Georgia, August 15-18, 2021.

Di Giulio, G., Hailemikael, S., Vassallo, M., and Milana, G. (2021). "EGS6 Blind prediction. Step1 by INGV and ENEA team". ESG6, Kyoto, Japan.

Hailemikael, S., Di Giulio, G., Bordoni, P., Vassallo, M., Milana, G. (2021) "ESG6 Blind prediction. 1D modeling for steps 2 and 3 by INGV and ENEA team", ESG6, Kyoto, Japan.

Hase, Y. and Iwauchi, A., (1992). "On Cyclocarya paliurus (Batal.) Iljinskaja from the Early and Middle Pleistocene Sediments in Central Kyushu, Japan". 熊本大学教養部紀要 自然科学篇, (27), pp.p 59-68.

Ishizaka S., Iwasaki, Y., Hase, Y., Watanabe, K., Iwauchi, A. and Taziri, M., (1995). "Subsidence Rate and Sediments of the Last Interglacial Epoch in the Kumamoto Plain, Japan", *The Quaternary Research*, **34** (5), 335-344.

Itasca Consulting Group, Inc. (2019). "FLAC3D — Fast Lagrangian Analysis of Continua in Three-Dimensions, Ver. 7.0". Minneapolis: Itasca.4.

Koketsu, K.,Miyake, H., andSuzuki, H., (2012). "Japan Integrated Velocity Structure Model Version 1", *Proc. World Conf. Earthq. Eng.*, Paper No. 1773.

Koketsu, K., Miyake, H., Afnimar, and Tanaka, Y. (2009). "A proposal for a standard procedure of modeling 3-D velocity structures and its application to the Tokyo metropolitan area, Japan", *Tectonophysics*, **472**, 290-300.

Nakazawa, T., Sakata, K., Sato, Y., Hoshizumi, H., Urabe, A., and Yoshimi, M. (2018). "Stratigraphy and distribution pattern of volcanogenic sediments beneath downtown Mashiki, Kumamoto, SW Japan, seriously damaged by the 2016 Kumamoto Earthquake", *Jour. Geol. Soc. Japan*, **124**, 5, 347–359, doi: 10.5575.

Oyo Corporation (2020) Kumamoto Eq. Ground Structure Survey Report (Draft).

Tsuno, S., Korenaga, M., Okamoto, H., Yamanaka, H., Chimoto, K., and Matsushima, T. (2017). "Local site effect in Kumamoto City revealed by the 2016 Kumamoto earthquake", *Earth, Planets and Space*, **69**, 37, doi 10.1186/s40623-017-0622-6.

Investigation and Observation for Elucidation of Three-Dimensional Shape of 3.2 Fault Zone and Crustal Structure around Fault Zone 3.2 -1 Investigation and Observation for Elucidation of Crustal Structure by Earthquake, Electromagnetic, etc.
https://www.jishin.go.jp/main/chousakenkyuu/kumamoto_sogochousa/h28/h28kumamoto_sogochousa_3_2.pdf

"Seamless Digital Geological Map of Japan (1:200,000) by National Institute of Advanced Industrial Science and Technology (AIST)" (https://gbank.gsj.jp/seamless/index_en.html?).

FIGURES

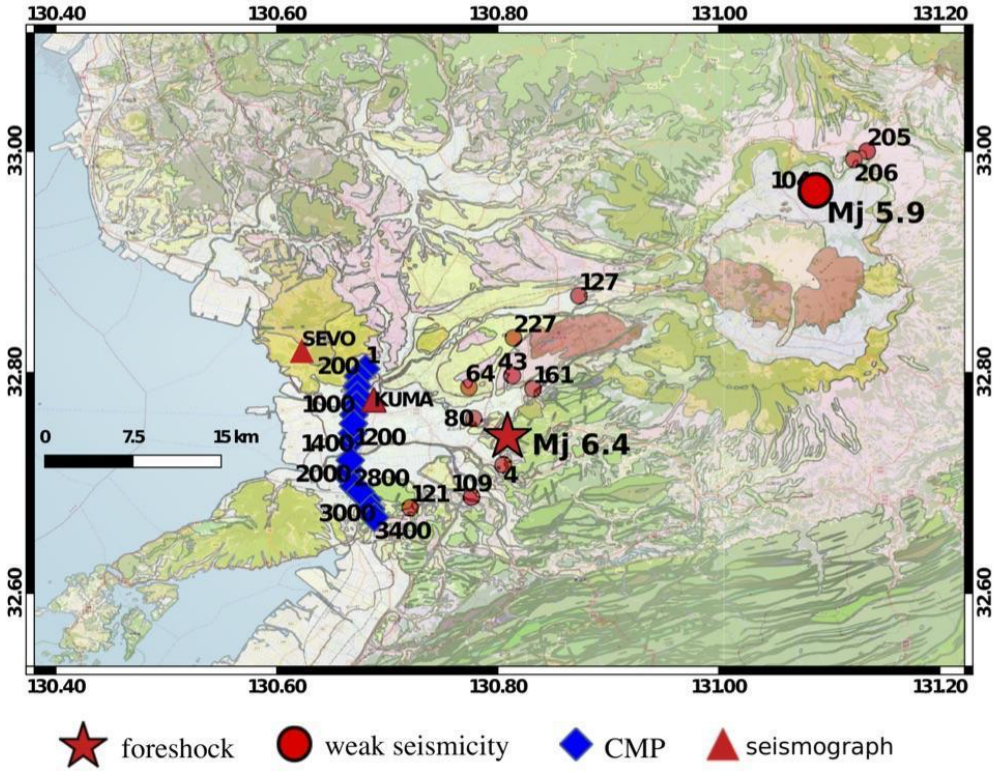

Figure 1. Geological map by AIST (https://gbank.gsj.jp/seamless/index_en.html?) of the Kumamoto Prefecture area. Note the prediction site KUMA and the reference site SEVO (red triangles), the CMP of seismic reflection array (blue diamond).

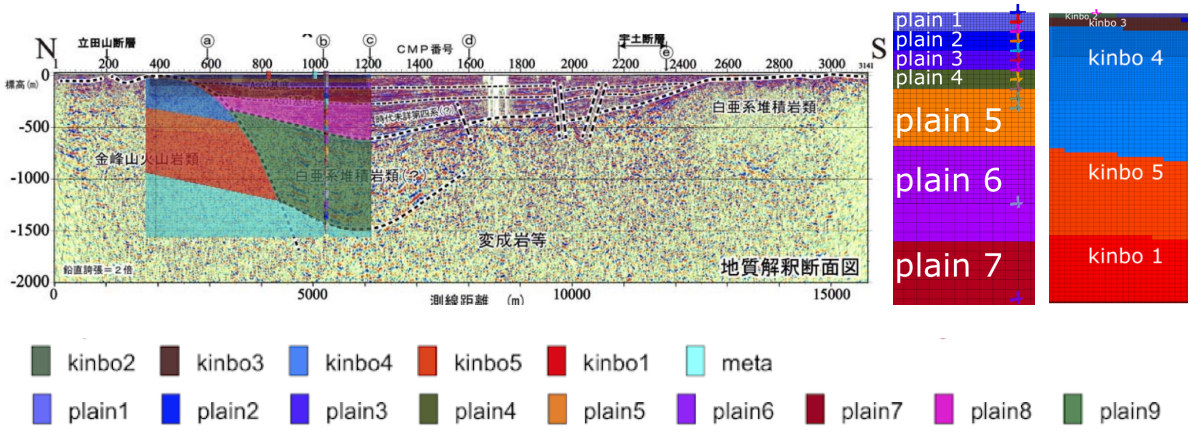

Figure 2. 2D Model geometry superimposed on the geological interpretation of the seismic reflection cross-section provided by CMPM. Target site is at CPb close to CMP 1000.

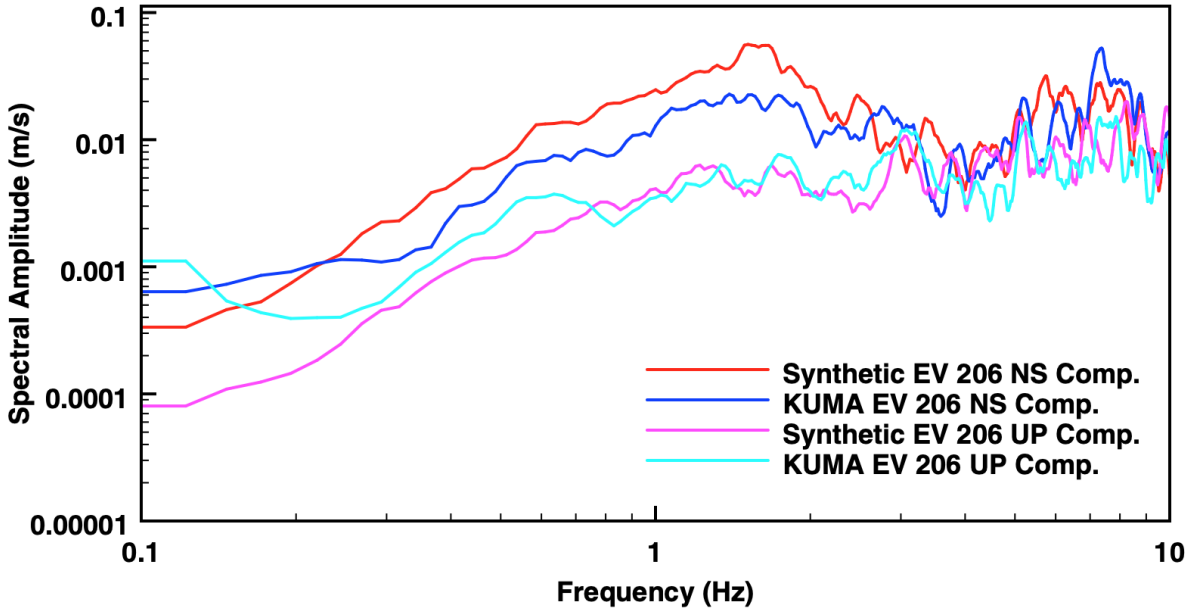

Figure 3. Comparison of Fourier spectra obtained by 2D simulation (Red and Magenta curves) and real data recorded at KUMA seismic station (Blue and Cyan) curves.

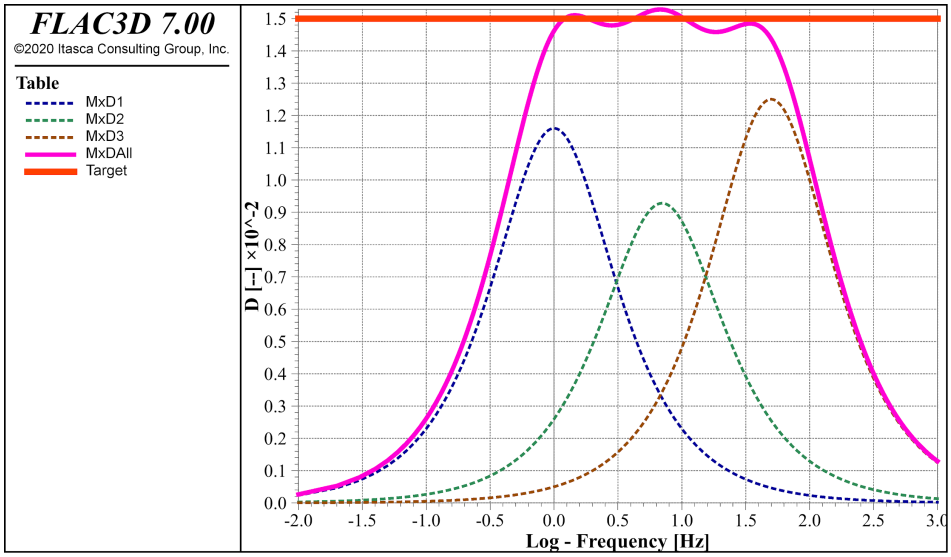

Figure 4. Maxwell damping curve for 1.5%.

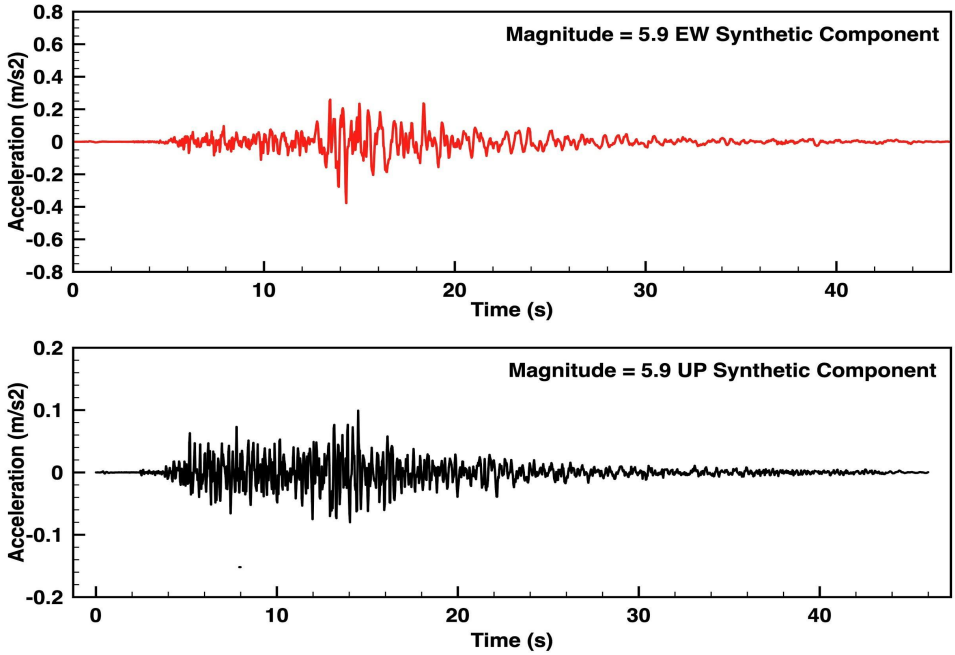

Figure 5. Horizontal and vertical component synthetic waveforms from the M=5.9 East-West and Up-Down component input.

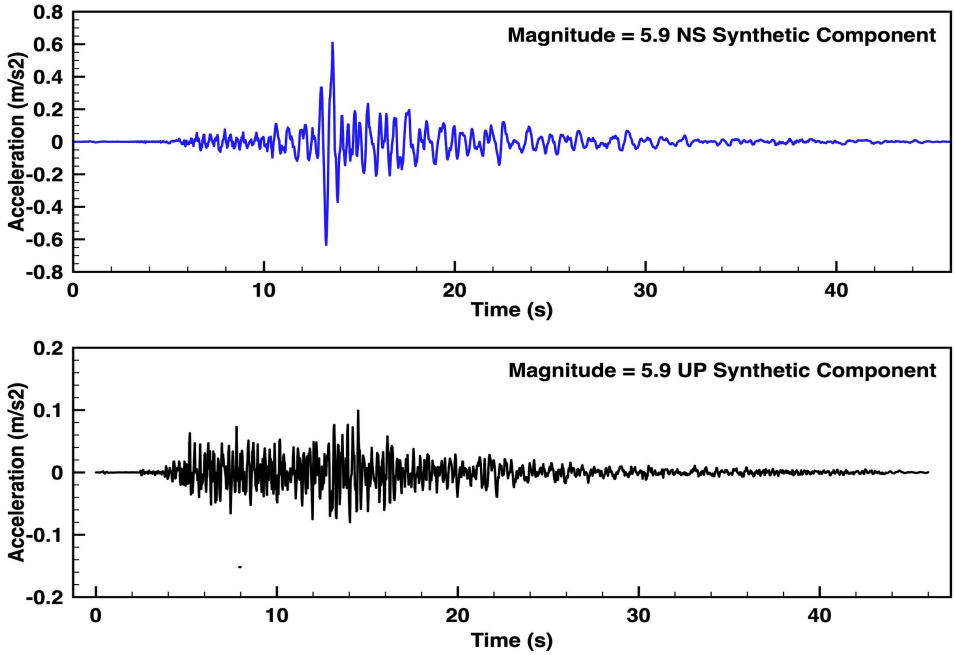

Figure 6. Horizontal and vertical component synthetic waveforms from the M=5.9 North-South and Up-Down component input.

.

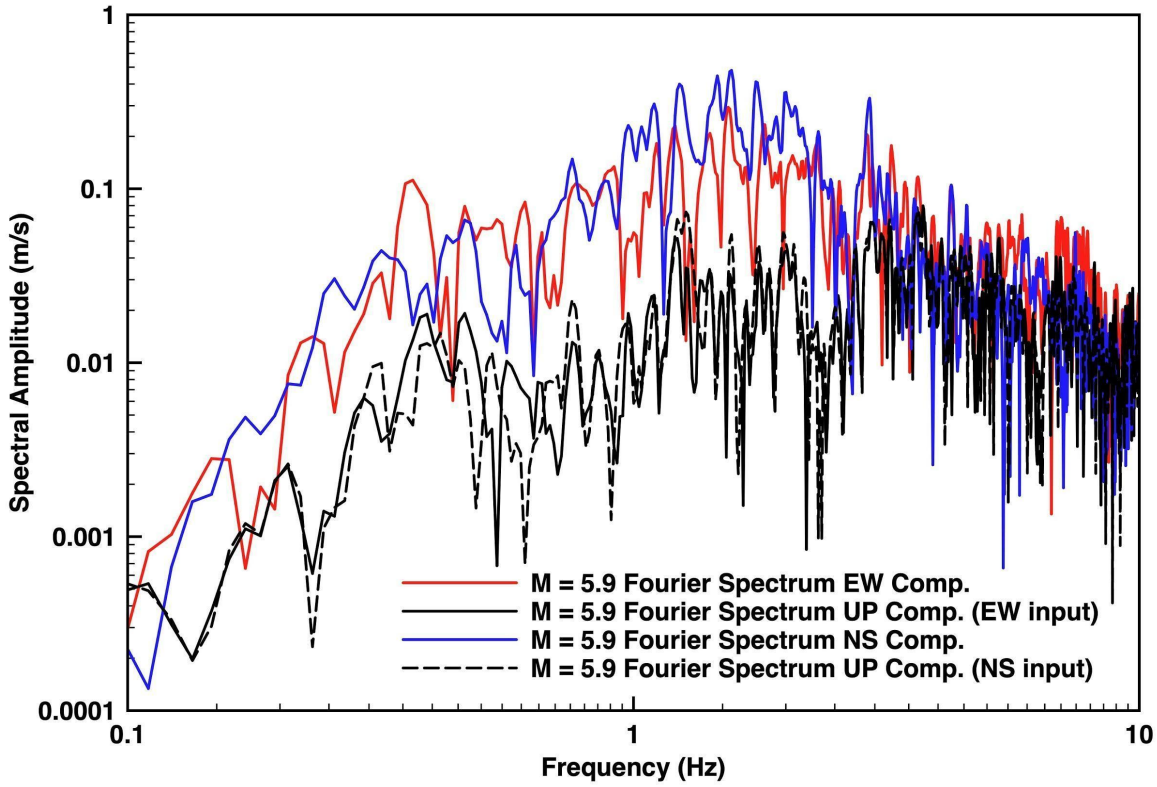

Figure 7. Fourier amplitude spectra of the synthetic waveforms of the horizontal and vertical component from the M=5.9 North-South (blue) East-West (red) and Up-Down (black).

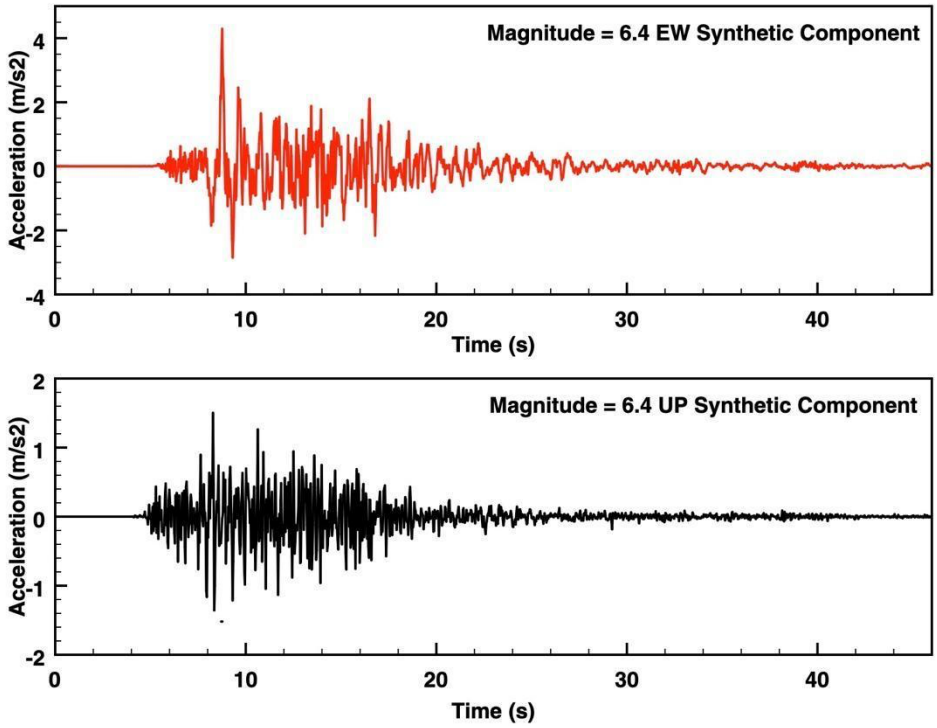

Figure 8. Horizontal and vertical component synthetic waveforms from the M=6.4 East-West and Up-Down component input.

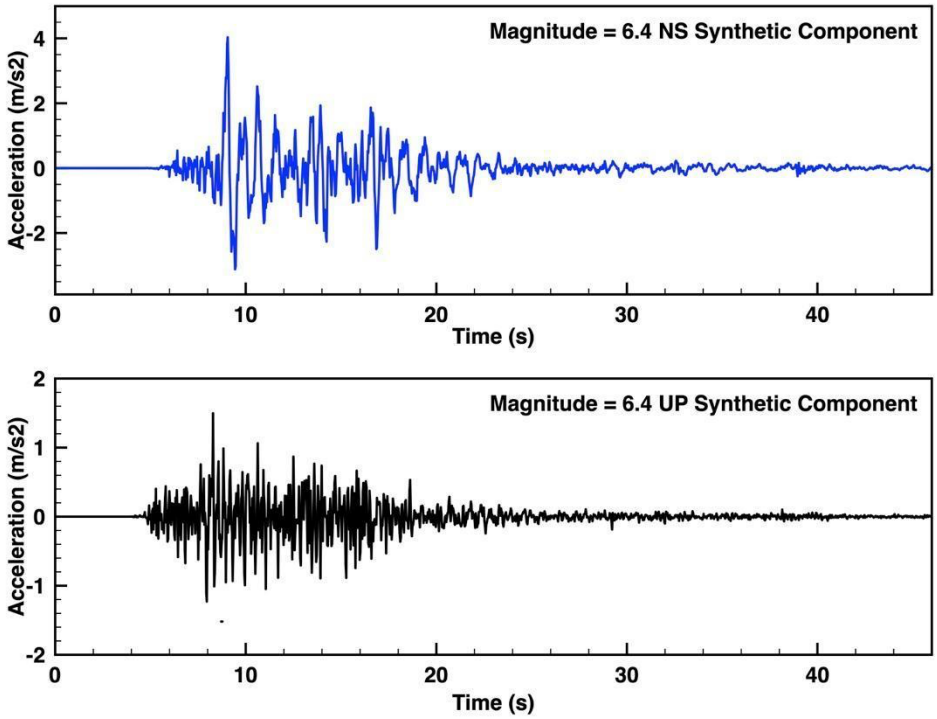

Figure 9. Horizontal and vertical component synthetic waveforms from the M=6.4 North-South and Up-Down component input.

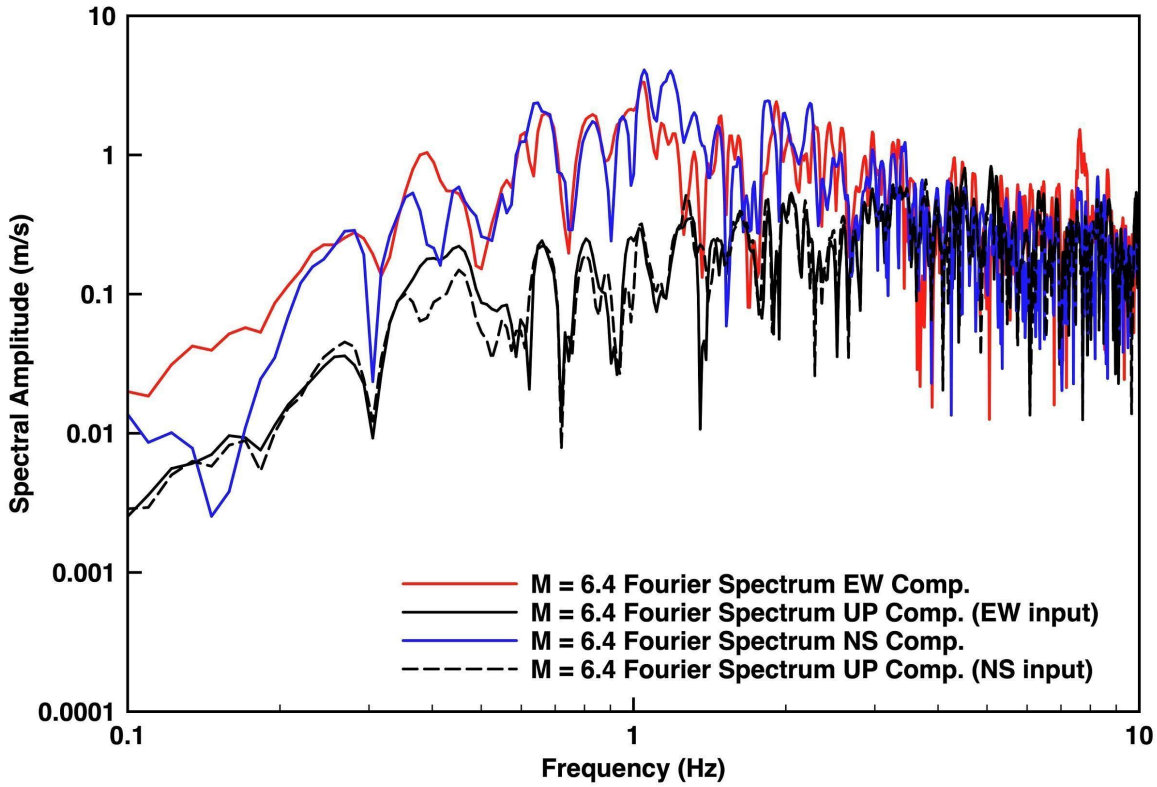

Figure 10. Fourier amplitude spectra of the synthetic waveforms of the horizontal and vertical component from the M=6.4 North-South East-West.

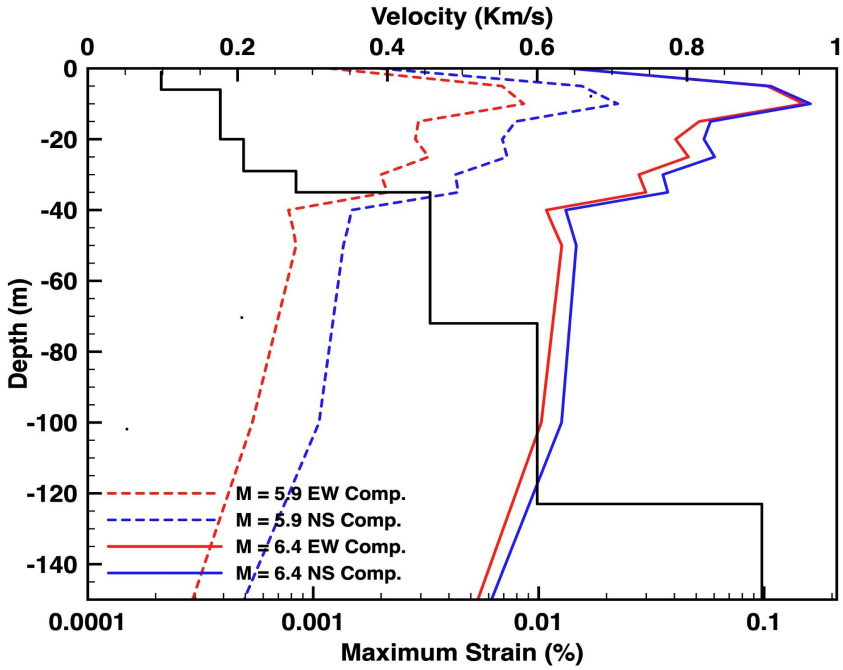

Figure 11. Comparison between shear velocity curve (black) and shear strain curves with depth, produced by the Mj=5.9 and Mj=6.4 events. The North-South component (in blue) reaches higher levels of strain than the East-West component (in red) at every depth. The highest level of strain - 0.02% for the Mj=5.9 and about 0.2% for the MJ=6.4 – is reached in the first 10 meters of depth in the second layer of the model.

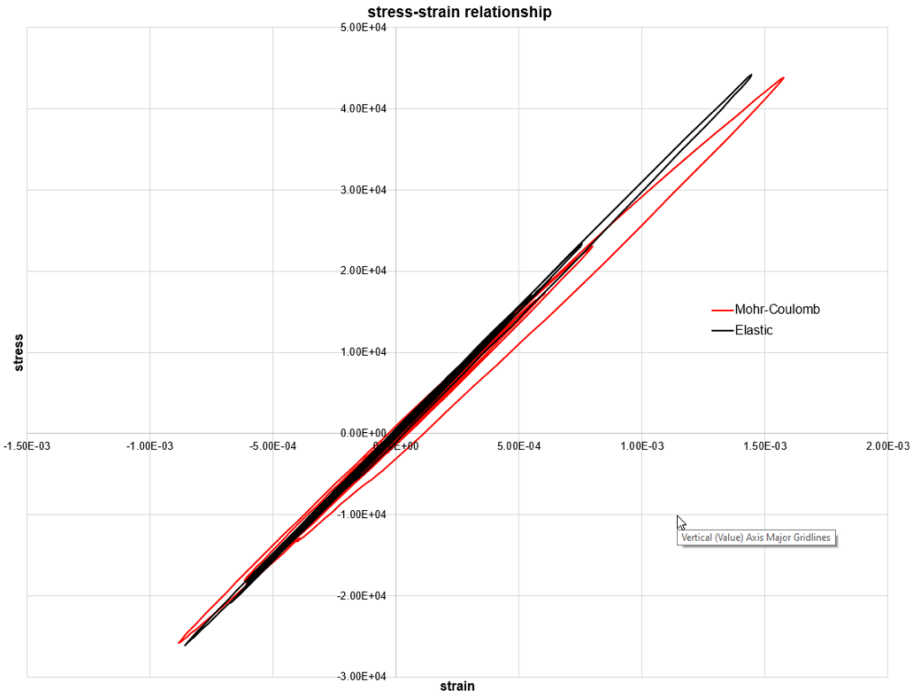

Figure 12. Comparison between stress-strain relationship during the Step 3 simulation for nonlinear Mohr-Coulomb constitutive model (red) and linear elastic constitutive model (black). See text more details about the additional parameters used in each simulation.

TABLES

Table 1

grid		1 densify from 0-200 m		2 densify from 0-100 m		3 densify from 0-60 m	
x-grid	y-grid	x-grid	y-grid	x-grid	y-grid	x-grid	y-grid
13	10	6.5	5	3.25	2.5	1.625	1.25

Table 2

H	Layer name	Vs	x-grid	y-grid	x-frequency	z-frequency
5.5	plain1	98	1.65	1.25	7.42	9.8
20	plain2	177	1.65	1.25	13.41	17.7
28.5	plain3	208	1.65	1.25	15.76	20.8
35	plain4	278	1.65	1.25	21.06	27.8
72.36	plain5	457	3.25	2.5	17.58	22.85
123.43	plain6	600	6.5	5	11.54	15
262.1	plain7	900	13	10	8.65	11.25
579.92	plain8	1100	13	10	10.58	13.75
1509.08	plain9	2100	13	10	20.19	26.25
1984.65	meta	3150	13	10	30.29	39.375

Table 3

Layer name	Depth (m)	Thickness (m)	Averaged CMPM Layers	Vp (m/s)	Vs (m/s)	Density (gr/cm3)	Damping	Poisson	PoissonFlac
plain1	0.00	5.5	1-2	398	98	1500	1.5%	0.46	0.45
plain2	5.5	14.5	3-4-5	1383	177	1590	1.5%	0.49	0.45
plain3	20	8.5	6-7-8	2585	208	1700	1.5%	0.5	0.45
plain4	28.5	6.5	9-10	1313	278	1700	1.5%	0.48	0.45
plain5	35	37.5	11-12-13	1643	457	1870	1.5%	0.46	0.45
plain6	72.0	51.0	14	2100	600	1900	1.5%	0.46	0.45
plain7	123.5	139.0	15	2400	900	2050	1.5%	0.42	0.42
plain8	262.5	318	16	2600	1100	2150	1.5%	0.39	0.39
plain9	580.5	929	17	4000	2100	2400	1.5%	0.31	0.31
meta	1509.5	∞	18-19	5500	3150	2600	1.5%	0.27	0.25

Table 4

FLAC3D Layer	JIVSM Layers	Vp (m/s)	Vs (m/s)	Density (gr/cm3)	Damping	PoissonFlac
kinbo2	1	1700	350	1800	1.5%	0.45
kinbo3	2	2000	500	2000	1.5%	0.45
kinbo4	5	2200	800	2070	1.5%	0.42
kinbo5	8	2700	1300	2200	1.5%	0.35
kinbo1	11	3500	2000	2350	1.5%	0.26
meta	∞	5500	3150	2600	1.5%	0.25

Table 5

Layer Name	Soil type	Cohesion (KPa)	Friction Angle	PI	OCR
plain1	silt + sand	10	32	20	4
plain2	sand	0	36	5	4
plain3	sand + silt	1	34	10	4

APPENDIX

For BP 4 we revised the output data sent by 14 of January 2021, as described in the following, and resubmitted them. In addition, we submitted a main-shock simulation output obtained using the same code, model geometry and mechanical parameters as STEP 2 and STEP3 fore-shock. Pictures included in the Extended abstract submitted by end of February 2021 had already been corrected for STEP3 A.1 point but they still had the polarity inverted.

STEP 2

1. We checked and inverted the polarity of the two horizontal components.
2. Fourier signals are the same as first submissions.

STEP 3

A. FORE-SHOCK
   1. We cut some pre-event signal and checked the timing of the first sample.
   2. We checked and inverted the polarity of the two horizontal components.
   3. Fourier signals are the same as first submissions.

B. MAIN-SHOCK
   1. We submitted the simulated synthetics (two horizontal components and two vertical components) from the main-shock and their Fourier amplitude spectra (Figure 1-3 this appendix).
   2. We cut the output after second 14.

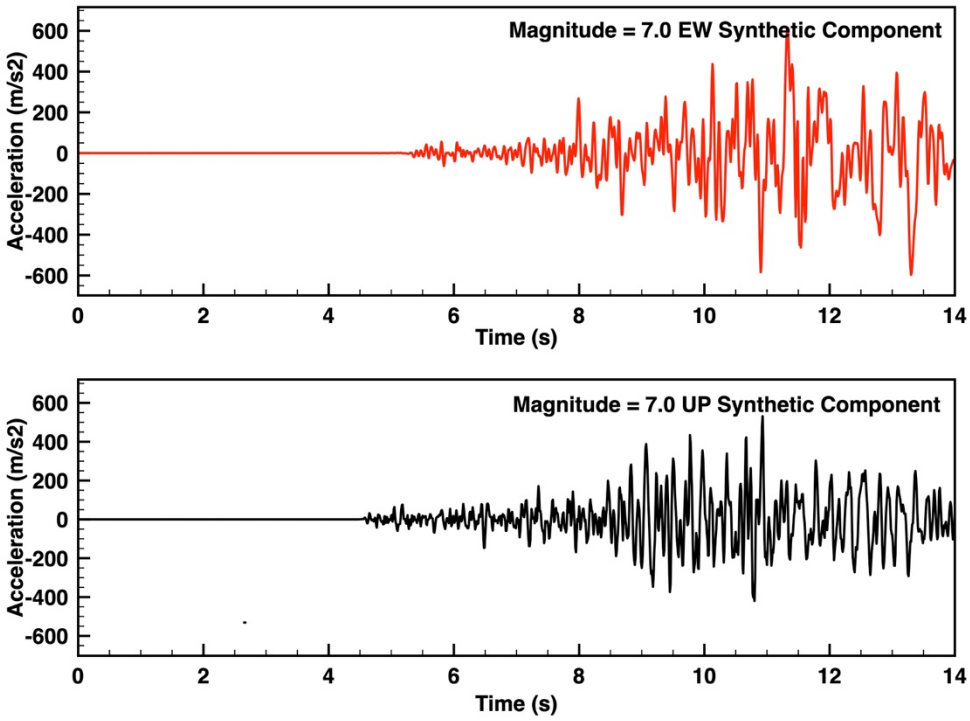

Figure 1. Horizontal and vertical component synthetic waveforms from the M=7-0 East-West and Up-Down component input.

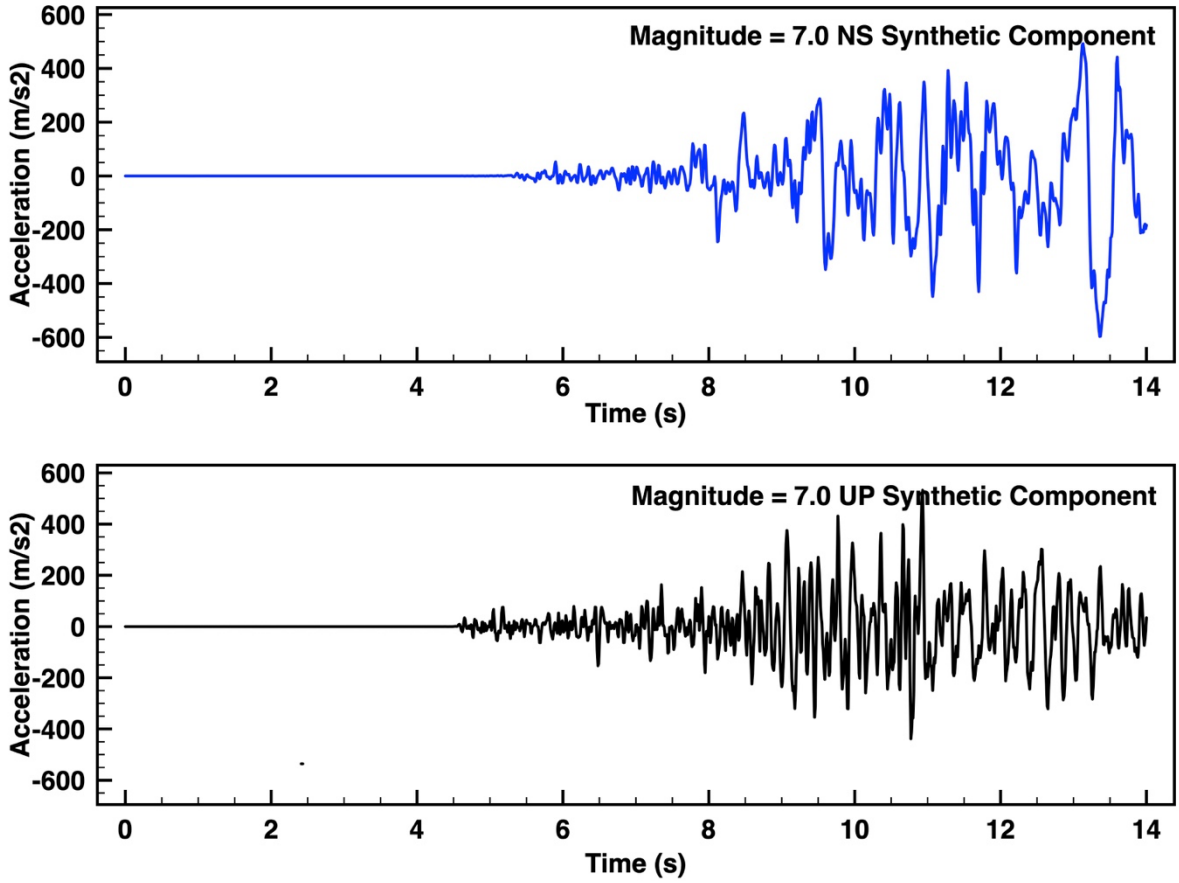

Figure 2. Horizontal and vertical component synthetic waveforms from the M=7.0 North-South and Up-Down component input.

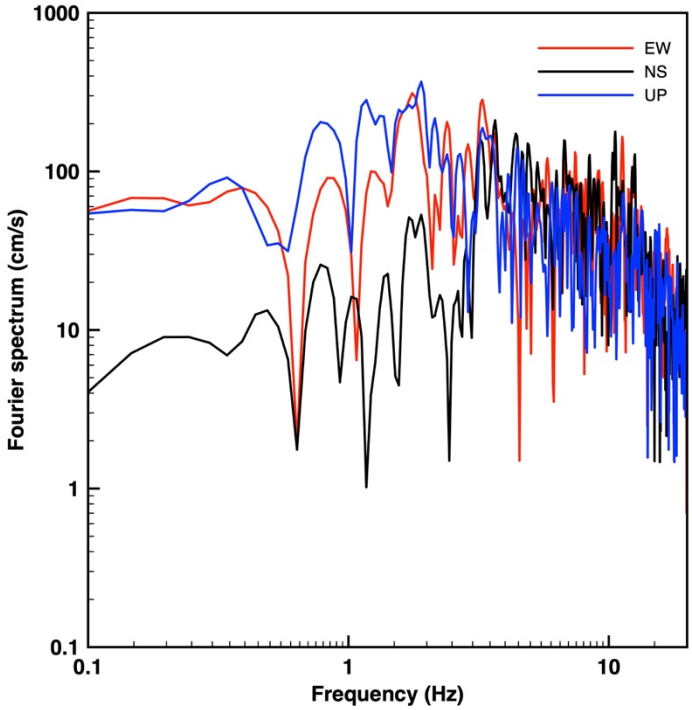

Figure 3. Fourier amplitude spectra of the synthetic waveforms of the horizontal and vertical component from the M=7.0 North-South (black) East-West (red) and Up-Down (blue).